In Situ and Nonvolatile Photoluminescence Tuning and Nanodomain Writing Demonstrated by All-Solid-State Devices Based on Graphene Oxide

Takashi Tsuchiya,* Tohru Tsuruoka, Kazuya Terabe, and Masakazu Aono

International Center for Materials Nanoarchitechtonics (WPI-MANA), National Institute for Materials Science (NIMS),1-1 Namiki, Tsukuba, Ibaraki 305-0044, Japan

ABSTRACT *In situ* and nonvolatile tuning of photoluminescence (PL) has been achieved based on graphene oxide (GO), the PL of which is receiving much attention because of various potential applications of the oxide (*e.g.*, display, lighting, and nano-biosensor). The technique is based on *in situ* and nonvolatile tuning of the sp^2 domain fraction to the sp^3 domain fraction (sp^2/sp^3 fraction) in GO through an electrochemical redox reaction achieved by solid electrolyte thin films. The all-solid-state variable PL device was fabricated by GO and proton-conducting mesoporous SiO_2 thin films, which showed an extremely low PL background. The device successfully tuned the PL peak wavelength in a very wide range from 393 to 712 nm, covering that for chemically tuned GO, by adjusting the applied DC voltage within several hundred seconds. We also demonstrate the sp^2/sp^3 fraction tuning using a conductive atomic force microscope. The device achieved not only writing, but also erasing of the sp^2/sp^3-fraction-tuned nanodomain (both directions operation). The combination of these techniques is applicable to a wide range of nano-optoelectronic devices including nonvolatile PL memory devices and on-demand rewritable biosensors that can be integrated into nano- and microtips which are transparent, ultrathin, flexible, and inexpensive.

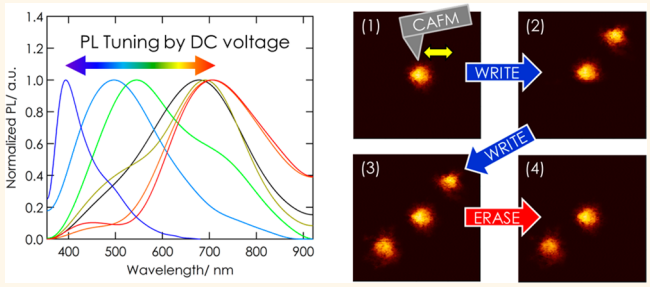

KEYWORDS: graphene oxide · solid state ionics · nanoionics · photoluminescence · band gap tuning

Graphene oxide (GO) has become a promising 2D material for exploring a variety of physical properties, including variable bandgap and transport properties, a wide energy range of photoluminescence (PL), and room-temperature ferromagnetism.[1−12] Recent investigations of the functions of GO revealed that the unique physical properties of GO strongly depend on the sp^2-hybridized conjugated domain to sp^3-hybridized domain (sp^2/sp^3) ratio, or the corresponding carbon/oxygen ratio (C/O).[4,13−19] Among the various functions of GO, PL in particular is receiving much attention in two distinct aspects: the mysterious bandgap dependence of the PL wavelength and the various potential applications. Intensive research on the bandgap and transport properties of chemically derived GO revealed that an increment in C/O due to hydrazine vapor evaporation narrows the bandgap, although the band edge is not well-defined.[4,5,13] On the other hand, the PL peak wavelength shifts toward the short wavelength side as C/O increases, which is completely opposite to the effect on the bandgap width.[6,20−22] This behavior defies the conventional emission mechanism, which is based on a recombination of electron−hole pairs generated at the conduction band minimum and valence band maximum, and has led to a vigorous discussion of various emission models based on the bond distortion in the GO,[7] the disorder-induced states and the small graphitic domains of the sp^2 cluster,[5,6] the quasi-molecular fluorophores,[23] the CO-related localized electronic state of oxidation sites,[24] the electronic transition between sp^2 regions and the boundary of oxidized carbon regions,[25] and

* Address correspondence to TSUCHIYA.Takashi@nims.go.jp, TERABE.Kazuya@nims.go.jp.

Received for review December 24, 2014 and accepted January 28, 2015.

Published online January 28, 2015
10.1021/nn507363g

the red-shifting process within a few picoseconds.[20] Although the origin of PL in GO is still open for further discussion, it is nevertheless promising for optoelectronic applications for several reasons. Fluorescence from low-cost organic compounds is of great importance for display and lighting applications.[26] The PL in GO has a wide range, from near-UV-to-blue (390 nm) to near-infrared (750 nm).[4−7] Furthermore, the stability of GO against photodegradation compared to conventional organic fluorophores is attractive for nano medicine applications. For example, biosensors that can selectively detect various biomolecules including pathogens and neurotransmitters have been achieved by using the PL in GO without the use of expensive antibodies.[27−29]

From the application viewpoint, bandgap tuning in GO is crucially important. The PL wavelength greatly varies with the bandgap; this variance is related to the oxygen atoms in the GO functional groups. The bandgap, or the extent of oxidation of the GO functional groups affects the charge transfer behavior in the biomolecule detection process by tuning of the relative potential energies in GO. While the bandgap is usually controlled using a chemical method, thermal annealing, or a plasma treatment,[4,13−18] we recently reported bandgap tuning through redox reaction using a solid electrolyte thin film.[19] With this technique, the bandgap can be tuned by simply applying DC voltage, and the complete process occurs within an all-solid-state device.[19] Accordingly, application of this technique to PL should lead to a new class of optoelectronic device enabling *in situ* and nonvolatile PL wavelength tuning. Here, we report the development and testing of an all-solid-state variable wavelength PL device based on solid state ionics.[30−32] We also report a technique for repeatedly writing and erasing bandgap tuned nanodomains using a conductive atomic force microscopy (CAFM) cantilever. The combination of these techniques is applicable to a wide range of nano-optoelectronic devices including nonvolatile PL memory devices and on-demand rewritable biosensors that can be integrated into nano- and microtips which are transparent, ultrathin, flexible, and low cost.

RESULTS AND DISCUSSION

PL Emission Property of GO and Solid Electrolytes. Prior to a discussion of a PL device fabricated using GO and solid electrolyte, we discuss the PL emission property of GO with different oxidation states as this property was an important factor in deciding which material to use for device development. The oxidation state was modulated by hydrazine vapor treatment. The normalized PL spectra in Figure 1A for pristine GO (a), GO reduced by exposure to hydrazine vapor for 3 min (b), and GO reduced by exposure to hydrazine for 10 min (c) clearly show that the peak wavelength shifted toward the short wavelength side as reduction proceeded from time a to time c. This behavior agrees well ones previously reported.[6,20−22] Figure 1B shows the PL spectra for three proton-conducting solid electrolyte thin films along with the PL spectra for time points a−c. Both yttrium stabilized zirconia (YSZ) and Nafion polymer thin films showed an intense PL emission that concealed the comparably weak PL from the three types of GO, particularly those from the two reduced GO (rGO) types with their very weak PL emissions.

Note that rGO is defined here as relatively reduced GO rather than GO in its initial state and that rGO has a wide range of PL, bandgap, and conductivity depending on the oxidation state (*i.e.*, C/O). In contrast to the two electrolytes, a mesoporous SiO_2 thin film showed extremely weak PL emission due to the low concentration of electronic defects, which work as a luminescent center. To observe the weak PL from the rGO in the device structure, the selection of low luminescent electrolyte is very important. We thus used mesoporous SiO_2 thin film as the electrolyte.

Fabrication of the All-Solid-State PL Source. The all-solid-state PL source we used is schematically shown in Figure 1C. It was fabricated of GO and mesoporous SiO_2 thin film by using spin coating, sol−gel method with template organics,[33] electron beam deposition, and so on. Please refer to methods for details on device fabrication. A high-resolution transmission electron microscope (HR-TEM) image of the GO/mesoporous SiO_2 thin film interface is shown in Figure 1D. The internal pore diameter was estimated to about 3.3 nm. The XRD pattern shown in Figure 1E agrees with that of a two-dimensional hexagonal mesostructure (*p6mm*) with *d*(100) of 3.752 nm.[34,35] The absence of (110) reflection, which is typically observed in the XRD pattern of a hexagonal structure, was due to the orientation of the hexagonal unit cell with the *c* and *a* axes parallel to the film substrate, which is evident in the field-emission scanning electron microscopy (FE-SEM) image shown in Figure 1F.[35] The internal pore diameter and wall thickness were determined to be 3.3 and 1.0 nm, respectively, on the basis of the FE-SEM, XRD, and HR-TEM observations.[36] About 10 layers of graphene sheets were observed in the GO layer (see inset in Figure 1D) and the average interlayer distance was 3.84 Å(d_{002}).[19] The GO layer showed intrinsic nanocurvature distortion in its two-dimensional single-crystalline structure, which is characteristic of multilayer graphene and GO.[37]

EDLT Using GO and Mesoporous SiO_2 Thin Film. An EDLT was fabricated of GO and mesoporous SiO_2 thin film and used to investigate the redox reaction of GO due to proton migration in mesoporous SiO_2 thin film. Figure 2 plots the electrical conduction characteristics (i_D, i_G *vs* V_G) of the EDLT at room temperature. The i_D and V_G are the current through the drain and the voltage between the gate and source, respectively. The abrupt jump and drop in i_D, indicated by black

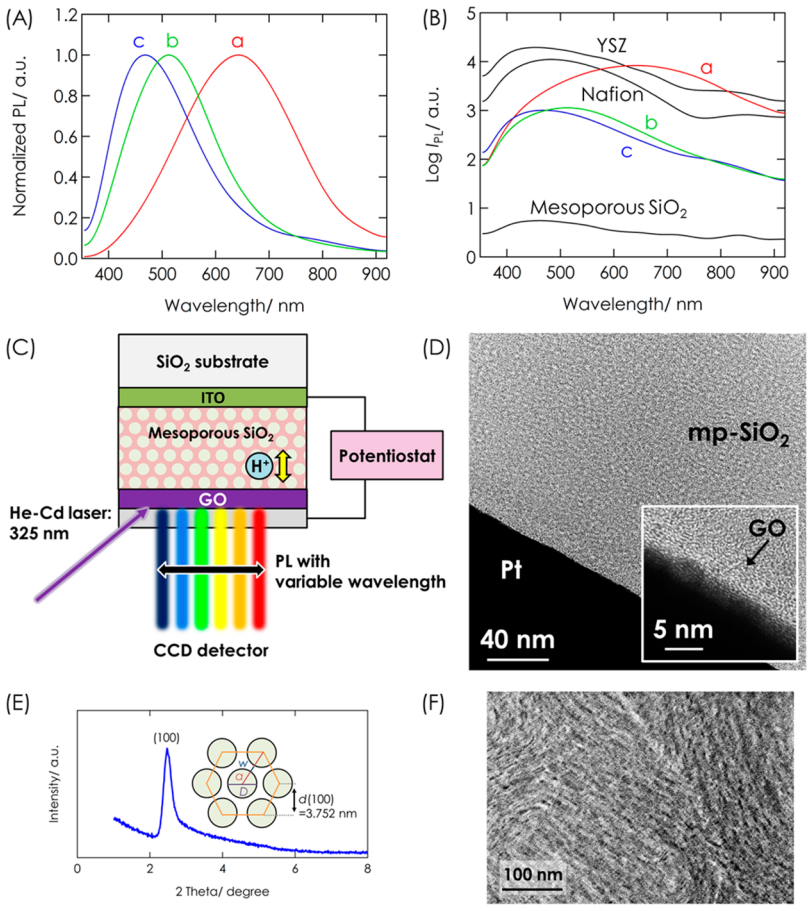

Figure 1. (A) Normalized PL spectra of three types of GO with different oxidation extents. Curves a, b, and c represent pristine GO, GO reduced by exposure to hydrazine vapor for 3 min, and GO reduced by exposure to hydrazine vapor for 10 min, respectively. (B) PL spectra of three proton-conducting solid electrolyte thin films (YSZ, Nafion, and mesoporous SiO_2). Three spectra in Figure 1A are also shown for comparison. (C) Schematic illustration of all-solid-state PL source made of GO and mesoporous SiO_2 thin film. (D) HR-TEM image of mesoporous SiO_2 (mp-SiO_2)/GO/Pt interface. Inset shows magnification of GO layers. (E) The XRD pattern of mesoporous SiO_2 thin film. (F) FE-SEM image of mesoporous SiO_2 thin film in surface view.

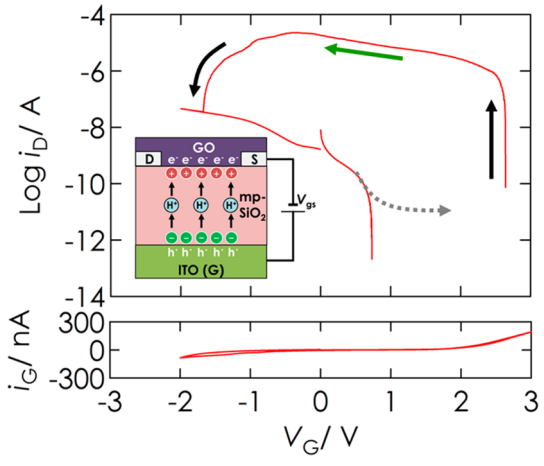

Figure 2. Electrical conduction characteristics of GO-based EDLT (schematically shown in inset) measured in air: i_D *vs* V_G (upper panel) and i_G *vs* V_G (lower panel). Sweep rate of V_G was 4 mV/s; V_D was 0.5 V.

arrows, are attributed to bandgap tuning in the GO due to redox reaction between the GO and rGO. The modulation in i_D indicated by the green arrow reflects an electrostatic carrier doping due to the EDL at the GO/mesoporous SiO_2 interface. Both of these behaviors agree well with that of a GO-EDLT previously fabricated using proton-conducting nanograined YSZ.[19,38] On the basis of the result, the redox reaction of GO can be safely achieved by proton migration in mesoporous SiO_2 thin film. Note that the fairly large i_D around 0 V is attributed to the transient EDL charging current between source and drain electrodes, and that the scale out of i_D in the V_G range of 0.7 to 2.6 V was due to overlapping between very large i_G and extremely small i_D (several tens of pA). The switching behavior was not significantly modulated even in a vacuum (about 1 Pa). The ON and OFF cycles can be safely repeated in 10 to 20 cycles depending on the voltage application hysteresis.

PL Tuning of the All-Solid-State PL Device Using GO and Mesoporous SiO_2 Thin Film. The PL tuning behavior of the device shown in Figure 1C upon DC voltage application was investigated. The polarity of *V* is defined as positive when GO is oxidized. Please see Methods for experimental details. The left panel of Figure 3A shows the

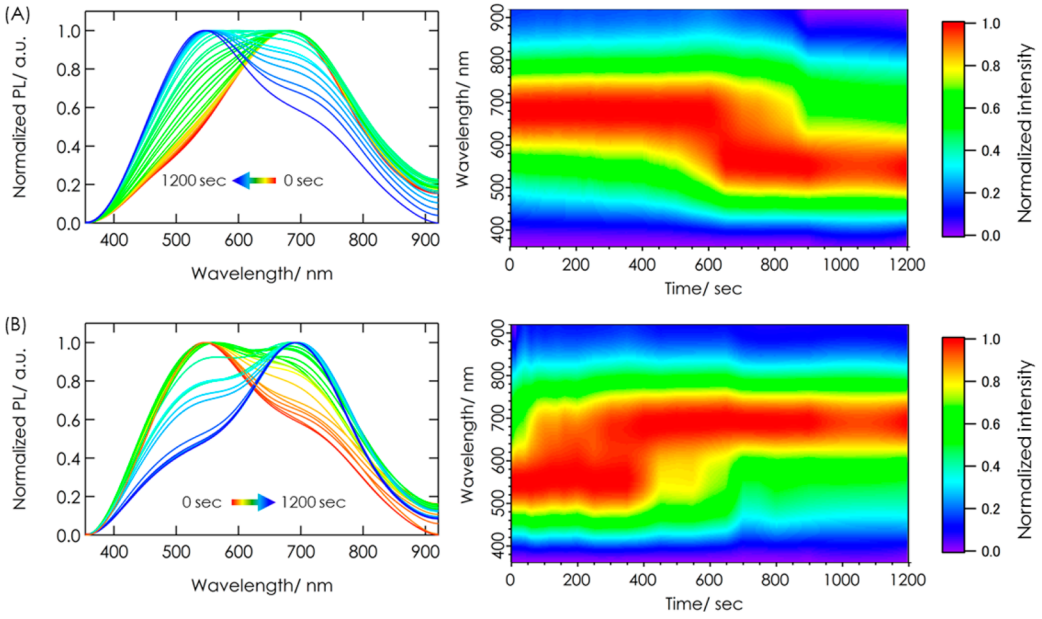

Figure 3. (A) (left) Variation in normalized PL spectra tuned by DC bias voltage application ($V = -2.5$ V) for 1200 s; (right) transition behavior of PL spectra with respect to time. (B) (left) Variation in normalized PL spectra tuned by subsequent application of opposite DC bias voltage ($V = 1.5$ V) for 1200 s; (right) transition behavior of PL spectra with respect to time.

variation in the normalized PL spectra tuned by DC bias voltage application ($V = -2.5$ V) for 1200 s. A broad emission peak at 676 nm was observed for the pristine GO. The peak shape agrees well with the PL spectra of GO containing a comparably large amount of oxygen (*e.g.*, carbon−carbon/carbon−oxygen bond ratio (C:O) of 0.85).[7,20] Upon a DC bias of −2.5 V, the emission peak became weak, and another peak appeared at 544 nm. Since PL energy modulation of GO in aqueous solution by the pH is known in addition to that by reduction and oxidation reaction of GO,[23,39] the pH modulation due to concentration polarization of protons in GO by the DC voltage application was also one possible mechanism for the PL tuning in the device. However, it should be volatile in contrast to the nonvolatile operation observed in the present result. Accordingly, the PL tuning is attributed to reduction and oxidation of GO. This second peak at 544 nm thus corresponds to emission from rGO electrochemically reduced *via* solid electrochemical reactions. The reactions are expressed as

$$C_xH_yO_z - OH + H^+ + e' \rightarrow C_xH_yO_z + H_2O \quad (1)$$

for the phenol group and as

$$C_xH_yO_z(=O) + 2H^+ + 2e' \rightarrow C_xH_yO_z + H_2O \quad (2)$$

for the epoxy, ketone, and carbonyl groups. The H^+ and e^- represent protons in the mesoporous SiO_2 thin film and electrons introduced from the metal electrode, respectively. Whereas the C/O ratio of the GO should increase for both reactions, the phenol, carbonyl, and epoxy groups were apparently the main reactants as shown by X-ray photoemission spectroscopy.[40]

The transition behavior of the PL spectra is shown in the right panel of Figure 3A. A broadening of the peak at 676 nm started at 390 s and finished at 640 s. The broadening was followed by a decrease of component at 676 nm and the variation in the spectra shape was finished within 900 s. The PL peak shift corresponds to the sp^2/sp^3 variation from 1.14 to 2.82, estimated on the basis of comparison with the result of X-ray photoemission spectroscopy.[40]

Figure 3B shows the variation in the spectra upon subsequent application of an opposite DC bias voltage of 1.5 V, which caused an electrochemical oxidation from rGO to GO. No significant difference was found in the reverse process except for a slightly sharpened peak shape on the long wavelength side and a small peak shift (from 676 to 690 nm). As shown in the right panel of Figure 3B, the transition behavior finished within 800 s, which is comparable to the 900 s in the reduction process. On the other hand, a broadening of the emission peak at 544 nm was observed at 40 s, which is almost one order earlier than the 390 s observed in the reduction process. Details of the transition behavior are discussed below based on CAFM measurement.

The decrease in the peak wavelength from the pristine condition (676 nm) to the reduced condition after DC bias voltage application (544 nm) was 132 nm, which is rather small with respect to the previous reports on chemically reduced GO.[4,6,7,20−22] Thus, we further investigated the effect of a DC bias voltage on the PL spectra and the peak wavelength. Figure 4 panels A and B show the DC bias dependence of the normalized PL spectra and peak wavelength tuned by various DC bias voltage applications for 1200 s. The peak wavelength in the reduction process was

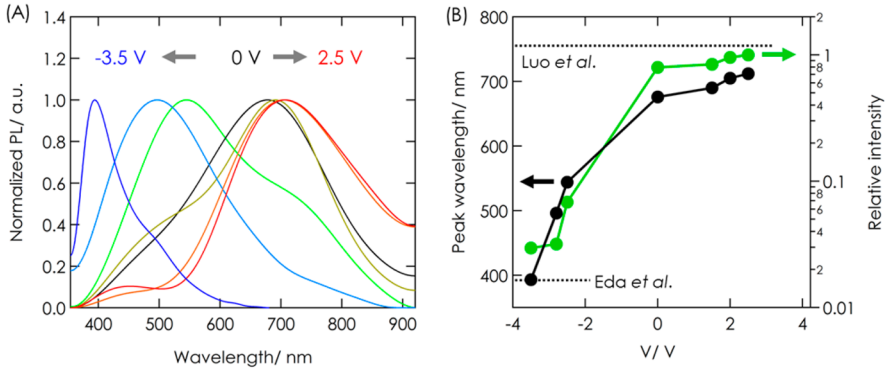

Figure 4. A) DC bias dependence of normalized PL spectra tuned by application of various DC bias voltages for 1200 s. B) DC bias dependence of peak wavelength (left axis, indicated by black circles) and relative intensity (right axis, indicated by green circles, indicated as value relative to intensity (with V = 2.5 V).

widely modulated, from 544 nm (V = −2.5 V) to 393 nm (V = −3.5 V). This behavior is qualitatively consistent with the considerable voltage dependence of the optical bandgap in the reduction process, which was previously investigated using the UV−vis−NIR reflectance measurement.[19] Note that the GO bandgap can be a measure of the extent of reduction (*i.e.*, C/O), while the bandgap does not correspond to the PL emission energy as mentioned above.[6,20−22] The peak wavelength of 393 nm with V = −3.5 V agrees well with 390 nm for extensively reduced GO.[4]

The peak wavelength in the oxidation process was not significantly altered even though the bias voltage was varied from 1.5 V (690 nm) to 2.5 V (712 nm). The longest peak wavelength of 712 nm (with V = 2.5 V) is 38 nm shorter than the reported peak wavelength of 750 nm.[7] This means that the short wavelength extreme of PL in GO is covered by the proposed PL tuning technique while the long wavelength extreme is slightly out of range. This indicates that the oxidation atmosphere created in the GO by the proposed technique is somewhat weaker than those created using other chemical methods.

Figure 4B also shows the relative intensity of the PL emission at the peak wavelength under various DC bias voltage conditions. The intensity with V = −3.5 V was almost two orders smaller than that with V = 2.5 V. Such a drastic change in PL intensity, or the corresponding quantum yield has been reported for rGO processed using chemical methods and photoreduction, and it can be understood as a quenching due to an increase in sp^2 domains in GO.[4,21] In one study, the decrease in PL intensity as reduction proceeds was reversed at a certain point in the reduction treatment, and the PL intensity resumed increasing.[21] On the basis of a detailed analysis of reduction kinetics, McDonald *et al.* assigned the reduction process in which the PL intensity decreases to the reduction process evolving the H_2O molecule, and assigned the subsequent PL intensity increase to that evolving the CO and CO_2 molecules.[21] The trend change, however, was not observed in the solid electrochemical reduction process in this study. Given the assignment by McDonald *et al.*, the absence of the trend change implies that a contribution from the solid electrochemical reduction evolving the CO and CO_2 molecule is comparably small. The feature may help the cyclability of the present technique that should be disturbed by carbon vacancy and dangling bond generation in the basal plane of GO, which is not completely annealed out even at 1273 K and is suggested to be hardly recovered in an electrochemical reaction at a temperature as low as room temperature.[11]

Since the origin of PL in GO and the peak shift mechanism are still open for discussion, various possible mechanisms for the PL tuning are to be considered. Among them, an alteration of the relative amount of functional groups may be an operation principle rather than the sp^2/sp^3 variation.[41] However, details of the PL tuning mechanism cannot be discussed on the basis of the present experimental results.

Nanodomain Writing and Erasing Using CAFM. The bandgap tuning using a solid electrochemical reaction can be extended to the writing and erasing of small rGO dots in the GO surface based on CAFM. The CAFM setups for bandgap tuning (i) and current imaging (ii) are illustrated in Figure 5. First, the insulating GO surface was reduced to conductive rGO by contact with a Pt−Rh cantilever with a tip voltage of −1.2 V (*vs* ITO electrode) for 0.5 s in setup (i). The rGO dots were imaged by passing a current through the cantilever scanning the surface with a tip voltage of −0.1 V (*vs* Au current collector). The first dot was written in the center of a 4 × 4 μm^2 working area by the process. The second and third dots were also written in the upper right and lower left of the working area by the same processes. Then, one of the rGO dots in the upper right was erased by oxidative scanning with a tip voltage of 1.5 V (*vs* ITO electrode) for 100 s. Each setup could be switched without changing the cantilever position. See the Methods section for details of the measurement.

Figure 6 panels A to D show current images of the GO surface obtained at each step of the process

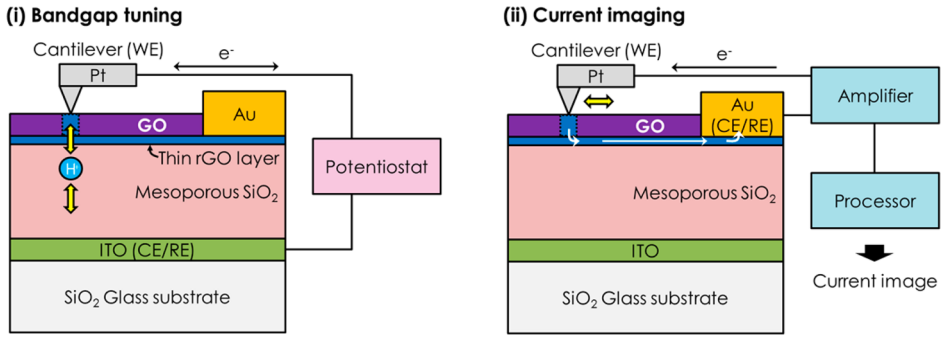

Figure 5. Schematic illustration of CAFM setups for bandgap tuning (i) and current imaging (ii). Thin rGO layer was inserted for current imaging (see Methods for details).

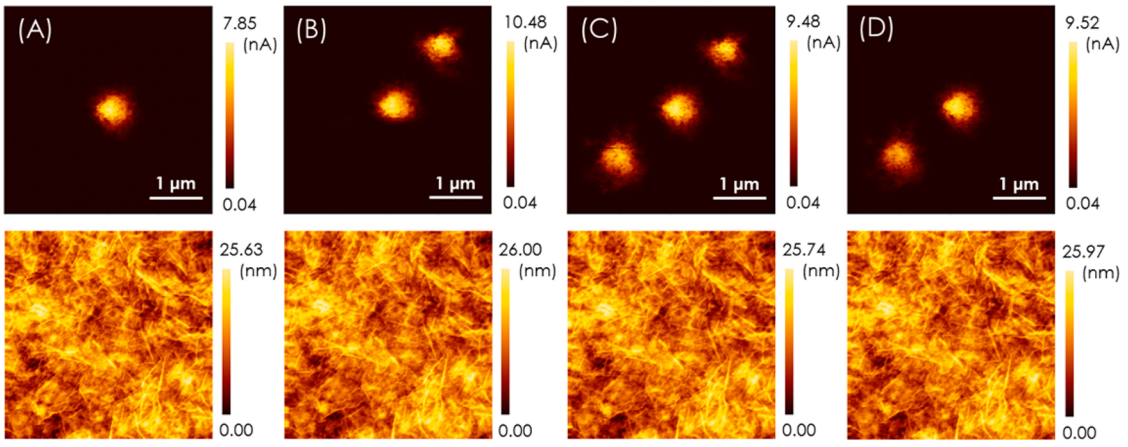

Figure 6. (A to D, top) CAFM images of rGO dots mapped by passing current through surface-scanning cantilever scanning with a tip voltage of −0.1 V (*vs* Au current collector) after writing of rGO dots. (A to D, bottom) Topography images obtained simultaneously with the current images.

described above. rGO dots with a diameter of 600 to 900 nm were written on the insulating GO surface although the edge of the dots was somewhat blurred. The resistance of the dots was estimated to be around 10 M ohms. After the dot was erased by oxidative scanning, the resistance at that point was very high, so that the point could not be distinguished from the pristine GO area (where the resistance exceeded 1 G ohms). Prolonged voltage application resulted in an rGO dot that was more conductive and larger, with a diameter of several micrometers. Topography images obtained simultaneously with the current images were also shown in Figure 6 panels A to D. Small ridges, or creaselike features were observed across the film. Such a morphology has been reported for multilayer graphene and GO.[42,43] A comparably large roughness was originated not only from GO but also from mesoporous SiO_2, which was slightly etched by the wet process. No significant difference was observed in the writing and erasing of rGO dots, although there was likely to have been small topographic modulation due to the expansion and shrinkage of the distance between the graphene sheets in the GO due to the redox reaction.[44−46] The height of the surface roughness prevented detecting such a small height modulation.

Whereas the reversible bandgap tuning phenomena between GO and rGO observed in the CAFM measurement is basically the same as that observed in the PL measurement and in the transistor property discussed above, an interesting feature was observed. The GO exhibited a spatially heterogeneous reactivity: several areas in the GO surface were barely reduced even after prolonged voltage application (up to 100 s) although the remaining areas were quickly reduced.

Concerning the spatially heterogeneous reactivity of GO, McDonald *et al*. investigated the time evolution of a 2D PL map of single layer GO under continuous laser irradiation.[21] Fluctuation in the local OH and the defect concentration in single layer GO causes spatially heterogeneous reactivity for photoreduction. The rate constant, however, differs by a factor of 2 at most, so the large heterogeneous reactivity observed in the present study is not attributed to fluctuations in the local OH and defects concentration.[21] We deduce that the heterogeneous reactivity was caused by a large potential drop near the GO/mesoporous SiO_2 interface due to the comparably rough surface (average roughness of 3.27 nm). Both proton transfer from mesoporous SiO_2 to GO and proton migration in GO may have been interrupted by the rough interface

caused by the GO wet-coating process. Such heterogeneous reactivity should have had a considerable effect on the kinetics in the PL tuning, during which the PL spectra were integrated within a laser spot 600 μm in diameter. We did not observe any part with difficulty for reduction/oxidation in the PL tuning experiments in contrast to the result for CAFM measurement. This is attributed to a much larger spot size for the PL experiment than the CAFM measurement. The difference between the two experiments indicated that the actual size and fraction of such an area with difficulty for reduction/oxidation are very small.

Related to the present technique, local anodic oxidation (LAO) of graphene using CAFM was previously reported.[47] Both directions operation (not only oxidation but also reduction) and a low operation voltage are major advantages of the proposed technique although a minimum width of modulated area is much greater than that in the LAO of graphene.

CONCLUSIONS

An all-solid-state PL device using GO and mesoporous SiO_2 enabling *in situ* and nonvolatile tuning of the PL wavelength was achieved on the basis of the solid state ionics principle. The PL peak wavelength can be tuned from 393 to 712 nm by adjusting the applied DC voltage between −3.5 and 2.5 V. This range covers that for chemically tuned GO except for near the long wavelength extreme (750 nm). The PL tuning can be completed within 800 s to 900 s, which is comparable to the time with chemical methods. Bandgap tuning in GO using CAFM was also achieved. The rGO dots can be written and erased within several hundred nanometers. While multilayer GOs with about 10 layers of graphene sheets were used in this study, a decrease in the layer number may effect the device performance. For instance, the switching speed for both PL tuning and nanodomain writing should be improved due to a decrease in the total amount of electric charges needed for the switching, while higher detectability in the measurement system will be needed. The improvement of switching speed may make this technique more suitable for practical applications.

The present technique should lead to a new class of nano-optoelectronic devices for display, lighting, and biosensing featuring *in situ* and nonvolatile operation. It should stimulate interest in the unique properties of graphene species and other various carbon materials (*e.g.*, carbon nanotubes, diamonds, fullerenes) from the viewpoint of application to multifunctional nanodevices.

METHODS

Fabrication of All-Solid-State PL Device Using GO and Mesoporous SiO_2 Thin Film. An all-solid-state PL device (shown schematically in Figure 1C) was fabricated on the flat surface of a SiO_2 substrate. A 200 nm-thick indium tin oxide (ITO) thin film was deposited by RF-sputtering. A 400 nm-thick mesoporous SiO_2 thin film was deposited using a sol−gel method with template organics.[34] First, 2.2 g of $CH_3(CH_2)_{15}N^+(CH_3)_3Br^-$ (CTAB) was dissolved in 30 mL of 1-C_3H_7OH at 90 °C. Next, 10 mL of $Si(OC_2H_5)_4$ (TEOS) was hydrolyzed for 1 h at 60 °C with 4 mL of 0.02 M HNO_3, 3.5 mL of 1-C_3H_7OH, and 4 mL of distilled water. The CTAB dissolved in 1-C_3H_7OH was added, and the solution was stirred for 1 h at room temperature. The precursor of mesoporous SiO_2 thin film was then deposited onto the ITO/SiO_2 substrate by spin coating the solution at a constant 3000 rpm. The spin-coated precursor was aged in air at room temperature for 48 h to evaporate the solvent and obtain CTAB ordering. The sample was then dried at 100 °C for 1 h and heated in air at 400 °C for 6 h to obtain mesoporous SiO_2 thin film. The mesopores structure with an internal pore diameter of about 3 nm is roughly parallel to the substrate as indicated in Figure 1 F. A 5.0-mg/mL GO aqueous solution containing one-atomic-layer of GO with a dimension of several hundred nanometers was spin-coated onto the mesoporous SiO_2 at a constant 2400 rpm and dried in air at 333 K for 1 h. The C/O for the GO was approximately 79/21. A 20 nm-thick Pt thin film was deposited onto the GO surface by electron beam deposition with a shadow mask.

PL Measurement. PL measurement was performed using the PL device and detection system schematically shown in Figure 1C. The 325 nm line of the He−Cd laser was used as the excitation source. While an excitation wavelength dependence of PL spectra was reported,[23,48] only the excitation wavelength was used. The power of the laser was limited to 10 μW to prevent photodegradation of the GO. The diameter of the measured spot area was 600 μm. The light emitted from the device was collected using achromatic lenses and then analyzed using a spectrograph equipped with a liquid-nitrogen-cooled charge-coupled device (CCD) detector. The detection system can efficiently operate over a spectral range of 380−900 nm. All the spectra shown here were corrected for the wavelength-dependent sensitivity of the photodetection system. The PL spectrum of the device in pristine condition was measured, and then a DC voltage of −2.5 V was applied to tune the PL peak wavelength. After the voltage application, the voltage was removed and the device was kept in an open-circuit condition for 20 s to prevent the spectrum modulation effect due to electric double layer generation by proton polarization at the interface. Then, PL measurement was performed to investigate the spectrum modulation effect from only nonvolatile bandgap tuning in the GO. The process ended when the time period of DC voltage application reached 1200 s. The process was then repeated in the same manner but with a DC voltage of 1.5 V. Twelve PL devices other than the devices shown in Figure 3 were tested to check the reproducibility of the PL tuning. The behavior of all devices was similar to the result shown in Figure 3.

Fabrication and Electrochemical Measurement of Electric Double Layer Transistor Using GO and Mesoporous SiO_2 Thin Film. An all-solid-state EDLT device (shown schematically in inset of Figure 2) was fabricated on the flat surface of a SiO_2 substrate. A 200 nm-thick indium tin oxide (ITO) thin film was deposited by RF-sputtering. A 400 nm-thick mesoporous SiO_2 thin film was deposited using a sol−gel method with template organics. First, 2.2 g of $CH_3(CH_2)_{15}N^+(CH_3)_3Br^-$ (CTAB) was dissolved in 30 mL of 1-C_3H_7OH at 90 °C. Next, 10 mL of $Si(OC_2H_5)_4$ (TEOS) was hydrolyzed for 1 h at 60 °C with 4 mL of 0.02 M HNO_3, 3.5 mL of 1-C_3H_7OH, and 4 mL of distilled water. The CTAB dissolved in 1-C_3H_7OH was added, and the solution was stirred for 1 h at room temperature. The precursor of mesoporous SiO_2 thin film was then deposited onto the ITO/SiO_2 substrate by spin coating the solution at a constant 3000 rpm. The spin-coated precursor was aged in air at room temperature for 48 h to evaporate the solvent and obtain CTAB ordering. The sample was then dried at 100 °C for 1 h and heated in air at 400 °C for 6 h to obtain mesoporous SiO_2 thin film. A 5.0-mg/mL GO aqueous solution containing one atomic-layer of GO with a dimension of several

hundred nanometers, was spin-coated onto the mesoporous SiO_2 at a constant 2400 rpm and dried in air at 333 K for 1 h. Source and drain Pt electrodes with tantalum oxide (Ta_2O_5) interlayer were deposited by RF sputtering with a shadow mask. The channel length and width were 75 and 50 μm, respectively. The ITO thin film was used as a gate electrode for electrochemical measurement. The electrochemical measurements were performed using a Keithley 4200-SCS parameter analyzer at room temperature.

Fabrication and Measurement of Bandgap Tuning in GO Using Conductive Atomic Force Microscopy. An all-solid-state device (shown schematically in Figure 5) was fabricated on the flat surface of a SiO_2 substrate. A 400 nm-thick mesoporous SiO_2 thin film was deposited using a sol–gel method with template organics. First, 2.2 g of $CH_3(CH_2)_{15}N^+(CH_3)_3Br^-$ (CTAB) was dissolved in 30 mL of 1-C_3H_7OH at 90 °C. Then, 10 mL of $Si(OC_2H_5)_4$ (TEOS) was hydrolyzed for 1 h at 60 °C with 4 mL of 0.02 M HNO_3, 3.5 mL of 1-C_3H_7OH, and 4 mL of distilled water. The CTAB dissolved in 1-C_3H_7OH was added, and the solution was stirred for 1 h at room temperature. The precursor of mesoporous SiO_2 thin film was then deposited onto the ITO/SiO_2 substrate by spin coating the solution at a constant 3000 rpm. The spin-coated precursor was aged in air at room temperature for 48 h to evaporate the solvent and obtain CTAB ordering. The sample was then dried at 100 °C for 1 h and heated in air at 400 °C for 6 h to obtain mesoporous SiO_2 thin film.

GO deposition/processing was then applied. A 5.0-mg/mL GO aqueous solution containing one-atomic-layer GO with a dimension of several hundred nanometers was spin-coated onto the mesoporous SiO_2 at a constant 4000 rpm and dried in air at 333 K for 1 h. This resulted in a thin GO layer comprising two or three graphene sheets. A 200 nm-thick Au thin film was deposited onto the GO surface by an electron beam deposition with a shadow mask. A DC voltage of −2.5 V was applied to the Au electrode for 30 min to reduce the GO near the Au electrode to rGO. This resulted in an rGO region within several hundred micrometers from the Au electrode. Additional GO spin coating was done onto the surface of the thin rGO layer at a constant 2400 rpm and dried in air at 333 K for 1 h. The surface-side GO was used for writing and erasing an rGO dot by bandgap tuning. The inserted thin rGO layer was used as an electronic current collecting layer for current imaging.

CAFM measurement was performed using a Nano Navi II E-sweep scanning probe microscope (SII Nanotechnology) in ambient atmosphere at room temperature. The spring constant of the conducting Pt–Rh coated Si cantilever (Omicron Nanotechnology Japan) was 0.2 N/m. For current imaging, a tip voltage of −0.1 V was applied between the tip and Au current collector in setup (ii) in Figure 5. The surface of the device was scanned with the tip in the scanning frequency of 0.5 Hz. The rGO dots were mapped by passing a current through the tip. For bandgap tuning (writing an rGO dot), the tip was kept at the location, and a voltage of −1.2 V was applied between the tip and ITO electrode for 0.5 s in setup (i) in Figure 5. The rGO dot in the upper right in Figure 6C was erased by oxidative scanning with a tip voltage of 1.5 V (*vs* ITO electrode) for 100 s. The scan was performed in a square region (1 μm × 1 μm) with the rGO dot at the center.

Conflict of Interest: The authors declare no competing financial interest.

REFERENCES AND NOTES

1. Park, S.; Ruoff, R. S. Chemical Methods for the Production of Graphenes. *Nat. Nanotechnol.* **2009**, *4*, 217–224.
2. Robinson, J. T.; Perkins, F. K.; Wei, Z.; Sheehan, P. E. Reduced Graphene Oxide Molecular Sensors. *Nano Lett.* **2008**, *8*, 3137–3140.
3. Eda, G.; Fanchini, G.; Chhowalla, M. Large-Area Ultrathin Films of Reduced Graphene Oxide as a Transparent and Flexible Electronic Material. *Nat. Nanotechnol.* **2008**, *3*, 270–274.
4. Eda, G.; Mattevi, C.; Yamaguchi, H.; Kim, H.; Chhowalla, M. Insulator to Semimetal Transition in Graphene Oxide. *J. Phys. Chem. C* **2009**, *113*, 15768–15771.
5. Eda, G.; Lin, Y.; Mattevi, C.; Yamaguchi, H.; Chen, H.; Chen, I.; Chen, C.; Chhowalla, M. Blue Photoluminescence from Chemically Derived Graphene Oxide. *Adv. Mater.* **2010**, *22*, 505–509.
6. Chien, C.; Li, S.; Lai, W.; Yeh, Y.; Chen, H.; Chen, I.; Chen, L.; Chen, K.; Nemoto, T.; Isoda, S.; Chen, M.; Fujita, T.; Eda, G.; Yamaguchi, H.; Chhowlla, M.; Chen, C. Tunable Photoluminescence from Graphene Oxide. *Angew. Chem., Int. Ed.* **2012**, *51*, 6662–6666.
7. Luo, Z.; Vora, P. M.; Mele, E. J.; Johnson, A. T. C.; Kikkawa, J. M. Photoluminescence and Band Gap Modulation in Graphene Oxide. *Appl. Phys. Lett.* **2009**, *94*, 111909.
8. Eng, A. Y. S.; Poh, H. L.; Sanek, F.; Marysko, M.; Matejkova, S.; Sofer, Z.; Pumera, M. Searching for Magnetism in Hydrogenated Graphene: Using Highly Hydrogenated Graphene Prepared *via* Birch Reduction of Graphite Oxides. *ACS Nano* **2013**, *7*, 5930–5939.
9. Ambrosi, A.; Pumera, M. Precise Tuning of Surface Composition and Electron-Transfer Properties of Graphene Oxide Films through Electroreduction. *Chem.—Eur. J.* **2013**, *19*, 4748–4753.
10. Matsumoto, Y.; Koinuma, M.; Ida, S.; Hayami, S.; Taniguchi, T.; Hatakeyama, K.; Tateishi, H.; Watanabe, Y.; Amano, S. Photoreaction of Graphene Oxide Nanosheets in Water. *J. Phys. Chem. C* **2011**, *115*, 19280–19286.
11. Mattevi, C.; Eda, G.; Agnoli, S.; Miller, S.; Mkhoyan, K. A.; Celik, O.; Mastrogiovanni, D.; Granozzi, G.; Garfunkel, E.; Chhowalla, M. Evolution of Electrical, Chemical, and Structural Properties of Transparent and Conducting Chemically Derived Graphene Thin Films. *Adv. Funct. Mater.* **2009**, *19*, 2577–2583.
12. Kozawa, D.; Zhu, X.; Miyauchi, Y.; Mouri, S.; Ichida, M.; Su, H.; Matsuda, K. Excitonic Photoluminescence from Nanodisc States in Graphene Oxides. *J. Phys. Chem. Lett.* **2014**, *5*, 1754–1759.
13. Mathkar, A.; Tozier, D.; Cox, P.; Ong, P.; Galande, C.; Balakrishnan, K.; Reddy, A. L. M.; Ajayan, P. M. Controlled, Stepwise Reduction, and Band Gap Manipulation of Graphene Oxide. *J. Phys. Chem. Lett.* **2012**, *3*, 986–991.
14. Kaiser, A. B.; Gommez-Navarro, C.; Sundaram, R. S.; Burghard, M.; Kern, K. Electrical Conduction Mechanism in Chemically Derived Graphene Monolayers. *Nano Lett.* **2009**, *9*, 1787–1792.
15. Gao, W.; Alemany, L.; Ci, L.; Ajayan, P. M. New Insights into the Structure and Reduction of Graphite Oxide. *Nat. Chem.* **2009**, *1*, 403–408.
16. Wang, Y.; Shi, Z.; Huang, Y.; Ma, Y.; Wang, C.; Chen, M.; Chen, Y. Supercapacitor Devices Based on Graphene Materials. *J. Phys. Chem. C* **2009**, *113*, 13103.
17. Loh, K. P.; Bao, Q. L.; Eda, G.; Chhowalla, M. Graphene Oxide as a Chemically Tunable Platform for Optical Applications. *Nat. Chem.* **2010**, *2*, 1015–1024.
18. Yang, D.; Zhou, L.; Chen, L.; Zhao, B.; Zhang, J.; Li, C. Chemically Modified Graphene Oxides as a Hole Transport Layer in Organic Solar Cells. *Chem. Commun.* **2012**, *48*, 8078–8080.
19. Tsuchiya, T.; Terabe, K.; Aono, M. In Situ and Non-volatile Bandgap Tuning of Multilayer Graphene Oxide in an All-Solid-State Electric Double-Layer Transistor. *Adv. Mater.* **2014**, *26*, 1087–1091.
20. Exarhos, A. L.; Turk, M. E.; Kikkawa, J. M. Ultrafast Spectral Migration of Photoluminescence in Graphene Oxide. *Nano Lett.* **2013**, *13*, 344–349.
21. McDonald, M. P.; Eltom, A.; Vietmeyer, F.; Thapa, J.; Morozov, Y. V.; Sokolov, D. A.; Hodak, J. H.; Vinodgopal, K.; Kamat, P. V.; Kuno, M. Direct Observation of Spatially Heterogeneous Single-Layer Graphene Oxide Reduction Kinetics. *Nano Lett.* **2013**, *13*, 5777–5784.
22. Chuang, C.-H.; Wang, Y.-F.; Shao, Y.-C.; Yeh, Y.-C.; Wang, D.-Y.; Chen, C.-W.; Chiou, J. W.; Ray, S. C.; Pong, W. F.; Zhang, L.; Zhu, J. F.; Guo, J. H. The Effect of Thermal Reduction on the Photoluminescence and Electronic Structures of Graphene Oxides. *Sci. Rep.* **2014**, *4*, 4525.
23. Galande, C.; Mohite, A. D.; Naumov, A. V.; Gao, W.; Ci, L.; Ajayan, A.; Gao, H.; Srivastava, A.; Weisman, R. B.; Ajayan, P. M.

Quasi-Molecular Fluorescence from Graphene Oxide. *Sci. Rep.* **2011**, *1*, 85–89.
24. Gokus, T.; Nair, R. R.; Bonetti, A.; Bö hmler, M.; Lombardo, A.; Novoselov, K. S.; Geim, A. K.; Ferrari, A. C.; Hartschuh, A. Making Graphene Luminescent by Oxygen Plasma Treatment. *ACS Nano* **2009**, *3*, 3963–3968.
25. Shang, J.; Ma, L.; Li, J.; Ai, W.; Yu, T.; Gurzadyan, G. G. The Origin of Fluorescence from Graphene Oxide. *Sci. Rep.* **2012**, *2*, 792–799.
26. Sheats, J. R.; Antoniadis, H.; Hueschen, M.; Leonard, W.; Miller, J.; Moon, R.; Roitman, D.; Stocking, A. Organic Electroluminescent Devices. *Science* **1996**, *273*, 884.
27. Jung, J. H.; Cheon, D. S.; Liu, F.; Lee, K. B.; Seo, T. S. A Graphene Oxide Based Immuno-biosensor for Pathogen Detection. *Angew. Chem., Int. Ed.* **2010**, *49*, 5708–5711.
28. Zhao, X.-H.; Kong, R.-M.; Zhang, X.-B.; Meng, H.-M.; Liu, W.-N.; Tan, W.; Shen, G.-L.; Yu, R.-Q. Graphene-DNAzyme Based Biosensor for Amplified Fluorescence "Turn-On" Detection of Pb^{2+} with a High Selectivity. *Anal. Chem.* **2011**, *83*, 5062–5066.
29. Jeon, S.-J.; Kwak, S.-Y.; Yim, D.; Ju, J.-M.; Kim, J.-H. Chemically-Modulated Photoluminescence of Graphene Oxide for Selective Detection of Neurotransmitter by "Turn-On" Response. *J. Am. Chem. Soc.* **2014**, *136*, 10842–10845.
30. Funke, K. Solid State Ionics: From Michael Faraday to Green Energy—The European Dimension. *Sci. Technol. Adv. Mater.* **2013**, *14*, 043502.
31. Tsuchiya, T.; Terabe, K.; Aono, M. All-Solid-State Electric-Double-Layer Transistor Based on Oxide Ion Migration in Gd-Doped CeO_2 on $SrTiO_3$ Single Crystal. *Appl. Phys. Lett.* **2013**, *103*, 073110.
32. Tsuchiya, T.; Miyoshi, S.; Yamashita, Y.; Yoshikawa, H.; Terabe, K.; Kobayashi, K.; Yamaguchi, S. Room Temperature Redox Reaction by Oxide Ion Migration at Carbon/Gd-Doped CeO_2 Heterointerface Probed by an *In Situ* Hard X-ray Photoemission and Soft X-ray Absorption Spectroscopies. *Sci. Technol. Adv. Mater.* **2013**, *14*, 045001.
33. Li, H.; Nogami, M. Pore-Controlled Proton Conducting Silica Films. *Adv. Mater.* **2002**, *14*, 912–914.
34. Daiko, Y.; Kasuga, T.; Nogami, M. Proton Conduction and Pore Structure in Sol-Gel Glasses. *Chem. Mater.* **2002**, *14*, 4624–4627.
35. Alberius, P. C. A.; Frindell, K. L.; Hayward, R. C.; Kramer, E. J.; Stucky, G. D.; Chmelka, B. F. General Predictive Syntheses of Cubic, Hexagonal, and Lamellar Silica and Titania Mesostructured Thin Films. *Chem. Mater.* **2002**, *14*, 3284–3294.
36. Lu, Y.; Ganguli, R.; Drewien, C. A.; Anderson, M. T.; Brinker, C. J.; Gong, W.; Guo, Y.; Soyez, H.; Dunn, B.; Huang, M. H.; Zink, J. I. Continuous Formation of Supported Cubic and Hexagonal Mesoporous Films by Sol−Gel Dip-Coating. *Nature* **1997**, *389*, 364.
37. Fujimoto, H. Theoretical X-ray Scattering Intensity of Carbons with Turbostratic Stacking and AB Stacking Structures. *Carbon* **2003**, *41*, 1585–1592.
38. Miyoshi, S.; Akao, Y.; Kuwata, N.; Kawamura, J.; Oyama, Y.; Yagi, T.; Yamaguchi, S. Low-Temperature Protonic Conduction Based on Surface Protonics: An Example of Nanostructured Yttria-Doped Zirconia. *Chem. Mater.* **2014**, *26*, 5194–5200.
39. Kochmann, S.; Hirsch, T.; Wolfbeis, O. S. The pH Dependence of the Total Fluorescence of Graphite Oxide. *J. Fluoresc.* **2012**, *22*, 849–855.
40. Tsuchiya, T.; Terabe, K.; Aono, M. Micro X-ray Photoemission and Raman Spectroscopic Studies on Bandgap Tuning of Graphene Oxide Achieved by Solid State Ionics Device. *Appl. Phys. Lett.* **2014**, *105*, 183101.
41. Li, M.; Cushing, S. K.; Zhou, X.; Guo, S.; Wu, N. Fingerprinting Photoluminescence of Functional Groups in Graphene Oxide. *J. Mater. Chem.* **2012**, *22*, 23374–23379.
42. Weber, C. M.; Eisele, D. M.; Rabe, J. P.; Liang, Y.; Feng, X.; Zhi, L.; Müllen, K.; Lyon, J. L.; Williams, R.; Vanden Bout, D. A.; Stevenson, K. J. Graphene-Based Optically Transparent Electrodes for Spectroelectrochemistry in the UV−vis Region. *Small* **2010**, *6*, 184–189.
43. Wang, X.; Zhi, L.; Tsao, N.; Tomovic, Z.; Li, J.; Müllen, K. Transparent Carbon Films as Electrodes in Organic Solar Cells. *Angew. Chem., Int. Ed.* **2008**, *47*, 2990–2992.
44. Khurana, G.; Kumar, N.; Kotnala, R. K.; Nautiyal, T.; Katiyar, R. S. Temperature Tuned Defect Induced Magnetism in Reduced Graphene Oxide. *Nanoscale* **2013**, *5*, 3346.
45. Ju, H.-M.; Choi, S.-H.; Huh, S. H. Effects of the Oxidation Degree of Graphene Oxide on the Adsorption of Methylene Blue. *J. Kor. Phys. Soc.* **2010**, *57*, 1649–1652.
46. Huh, S. H. Thermal Reduction of Graphene Oxide. *Physics and Applications of Graphene—Experiments*; Mikhailov, S. Ed.; InTech: Rijeka, Croatia, 2011; ISBN: 978-953-307-217-3.
47. Masubuchi, S.; Arai, M.; Machida, T. Atomic Force Microscopy Based Tunable Local Anodic Oxidation of Graphene. *Nano Lett.* **2011**, *11*, 4542–4546.
48. Cushing, S. K.; Li, Ming; Huang, F.; Wu, N. Origin of Strong Excitation Wavelength Dependent Fluorescence of Graphene Oxide. *ACS Nano* **2014**, *8*, 1002–1013.